

Gulf Stream and Kuroshio Current are synchronized

Tsubasa Kohyama¹, Hiroaki Miura², and Shoichiro Kido²

Key points:

- Temperatures of two major ocean currents, one in the Atlantic and the other in the Pacific, are synchronized for decadal time scale
- This synchronization is covariability shared by the Pacific Decadal Oscillation and the Northern Annular Mode
- The existence of an oceanic annular mode is hypothesized, which has some implications for midlatitude extreme weather and climate change

Abstract. Sea surface temperatures (SSTs) of the Gulf Stream and the Kuroshio are shown to be synchronized for the decadal time scale. This synchronization, which we refer to as the Boundary Current Synchronization (BCS), is associated with meridional migrations of the atmospheric jet stream. The singular value decomposition (SVD) between SST and zonal wind shows that, within the context of known climate modes, BCS can be understood as the covariability shared by the Pacific Decadal Oscillation and the Northern Annular Mode. Nevertheless, because the SVD time series exhibit high correlations with the zonal-mean meridional SST difference between the subtropics and the midlatitudes, BCS can be understood more simply as an oceanic annular mode. Air temperature regressed on the BCS index exhibits a similar spatial pattern to temperature observed in July 2018.

Index terms: 3339 Ocean/atmosphere interactions

Keywords: Western Boundary Current, Jet Stream

1. Introduction

The two warm ocean currents, the Gulf Stream and the Kuroshio, are located in the western boundaries of the Atlantic and the Pacific Oceans, respectively, so they are referred to as the western boundary currents (WBCs) [Hogg and Johns, 1995]. Meanderings of WBCs and the associated sea surface temperature (SST) variations have long been known to affect local weather and climate in the coastal metropolitan areas, mainly because WBCs transport heat from the tropics to the extratropics and modulate cyclogenesis [Sanders, 1986] and low cloud formation [Young and Sikora, 2003]. More recently, high-resolution satellite observations helped reveal that heat released from WBCs have profound impacts on the entire troposphere [Minobe et al., 2008; Nakamura et al., 2015; Masunaga et al., 2018]. The Gulf Stream and the Kuroshio also serve as surface fingerprints of low-frequency natural climate variability (e.g.,

Atlantic Meridional Overturning Circulation [Zhang, 2008], Pacific Decadal Oscillation (PDO) [Mantua et al., 1997]), and thus, understanding WBCs have major implications for paleoclimatology [Yamamoto et al., 2004], climate modeling [Paul and Schäfer-Neth, 2003], and disentangling natural variability from the anthropogenic climate change [Wills et al., 2018].

The tight linkage between the Gulf Stream and the Kuroshio has never been discovered, however. More than a decade ago, a monograph by Kelly and Dong [2004] found a hint of the WBC covariability in the upper ocean heat content data. They estimated that 26% of heat content variations over the entire North Atlantic and Pacific were in phase. Nevertheless, because the data length and the spatial resolutions were limited at that time, it was difficult to detect a fine structure or a strong coherence of the two WBCs. Though some climatologists mentioned this potential WBC covariability as an outstanding issue [Kwon et al., 2010], their monograph is, to the best of our knowledge, the only observational effort that was taken to explore a possible linkage between the Gulf Stream and the Kuroshio.

In the present day, satellite-based high-resolution SST data records [Reynolds et al., 2007; Dee et al., 2011] have become long enough to begin thorough analyses in this vein. The SST distribution in early 2018 may initiate speculations about a linkage between the two WBCs (Fig. 1a). During this time span, SSTs near both of the WBC regions are warmer by about 3-5 °C than the temporal mean over the past four decades, which corresponds to 2-3 standard deviations. This simultaneous warm event would be rarely experienced by random chance. One could attribute these record-breaking warm currents partly to the increasing greenhouse gas forcing, but this explanation appears not to be the whole story as we shall see.

In this study, we identify that the regional-mean SSTs over the two ocean currents are synchronized for interannual to decadal time scales. Data and methods are described in the next section. In section 3, the synchronization of the WBCs is demonstrated based on observational data analysis, and the physical mechanism is investigated from two different viewpoints. In this section, we also discuss some implications for the northern hemispheric weather and climate. Concluding remarks are presented in section 4.

2. Data and Methods

Observed SST, 2-meter air temperature (July only), and zonal wind fields at 300 and 800 hPa are from the European Center for Medium range Weather Forecasting (ECMWF) ERA-Interim reanalysis data [Dee

¹Department of Information Sciences, Ochanomizu University, Tokyo, Japan.

²Department of Earth and Planetary Science, The University of Tokyo, Tokyo, Japan.

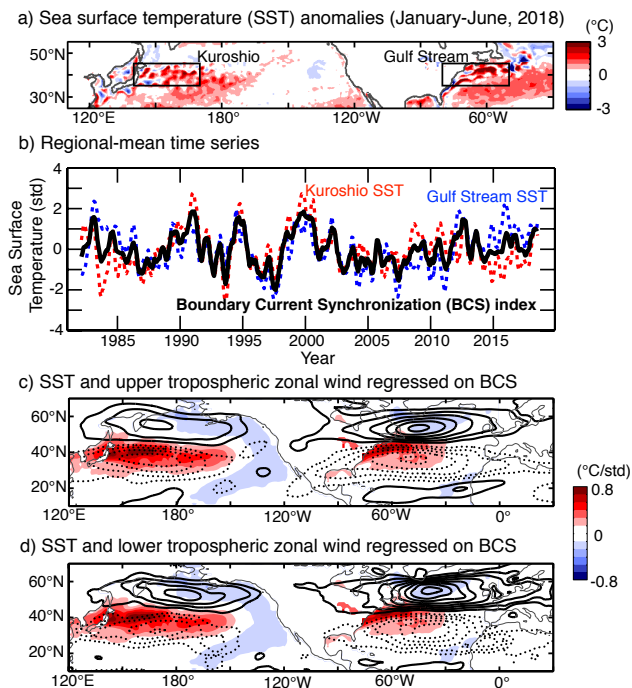


Figure 1. (a): Sea surface temperature (SST) anomalies averaged from January through June, 2018. Boxes show the locations of the two Western Boundary Currents (WBCs). (b): The BCS index (black) and five-month running-mean, standardized SST anomaly time series averaged over the Gulf Stream (35°N–45°N, 80°W–50°W) (blue dashed) and the Kuroshio (35°N–45°N, 140°E–170°E) (red dashed) regions defined as the boxes in (a). (c): Anomalies of SST (shaded areas) and zonal winds (contours) at 300 hPa regressed on the BCS index. Contour interval is 0.4 (m/s)/std. Solid (dashed) contours show positive (negative) anomalies, and zero contours are omitted. (d): As in (c), but for zonal winds at 850 hPa. Contour interval is 0.15 (m/s)/std.

et al., 2011] at <http://apps.ecmwf.int/datasets/data/interim-full-moda/levtype=sfc/>. The resolution is 1° in both longitudes and latitudes. The time span used in this study is from December 1981 through September 2018. To calculate detrended anomalies, we subtract monthly climatology (i.e., means of each calendar month) and linear trends. The Ssalto/Duacs altimeter products were produced and distributed by the Copernicus Marine and Environment Monitoring Service (CMEMS) (<http://www.marine.copernicus.eu>) and are used in this study for calculating the time series of sea level anomalies. The available time span of the sea level data is from 1993 to present. The ocean heat flux product is provided by the Woods Hole Oceanographic Institution (WHOI) Ocean-Atmosphere (OA) Flux project [Yu and Weller, 2007] available at <http://oaflex.whoi.edu/>. The time span of the heat flux data available is from 1984 through 2009.

In addition, because we need higher resolutions to make Fig. 1a, SST data for early 2018 with horizontal resolution of 0.25° is downloaded from the National Oceanic and Atmospheric Administration (NOAA) Optimum Interpolation SST (OISST) [Reynolds *et al.*, 2007] available at [https://www.esrl.noaa.gov/psd/data/gridded/data.](https://www.esrl.noaa.gov/psd/data/gridded/data.noaa.oisst.v2.highres.html)

[noaa.oisst.v2.highres.html](http://www.esrl.noaa.gov/psd/data/gridded/data.noaa.oisst.v2.highres.html). The monthly mean NAM index is downloaded from the Climate Prediction Center website (http://www.cpc.ncep.noaa.gov/products/precip/CWlink/daily_ao_index/ao_index.html), and the PDO index is from the website of the NOAA National Centers for Environmental Information (<https://www.ncdc.noaa.gov/teleconnections/pdo/>).

The statistical significance of correlations is tested by the two-tailed Student’s *t*-test. To estimate statistical degrees of freedom in auto-correlated time series, we employ a formula to calculate the effective sample size proposed by Bretherton *et al.* (1999) [Bretherton *et al.*, 1999].

3. Results

3.1. Boundary Current Synchronization (BCS)

Figure 1b shows the strong coherence of SST between the two warm currents. Here we plotted five-month running-mean, standardized time series of regional-mean SST anomalies over the Gulf Stream (35°N–45°N, 80°W–50°W) and the Kuroshio (35°N–45°N, 140°E–170°E) regions. The raw regional-mean time series exhibit a statistically significant correlation at the 95% confidence level. We hereafter investigate this phenomenon by referring to it as the Boundary Current Synchronization (BCS).

To represent the temporal BCS variability, the BCS index is defined as the average of the low-pass filtered, standardized regional-mean SST anomalies over the Gulf Stream (\tilde{G}) and the Kuroshio (\tilde{K}) regions, i.e., $BCS \equiv (\tilde{G} + \tilde{K})/2$ where a tilde denotes performing a one-year running-mean filter and then normalizing by its own standard deviation. The BCS index successfully explains the temporal SST variations of both the Gulf Stream and the Kuroshio regions.

The BCS index also captures the spatial distributions of the SST anomalies. Figures 1c and 1d show that meridional migrations of the tropospheric westerly jet stream through the entire troposphere serves as an essential component of BCS. In these figures, the regression maps of SST and zonal winds on the BCS index are presented. When the WBC regions are anomalously warm, both the upper (Fig. 1c) and lower (Fig. 1d) tropospheric jet streams tend to migrate northward, and vice versa.

Also shown in Fig. S1 is the same time series but for the sea level anomalies (i.e., a proxy of current strength), which exhibits some similarities to those of SST. Because net surface heat flux anomalies are not so coherent with SST and sea level (Fig. S1), wind-driven ocean dynamics, rather than thermodynamical processes, is suggested to be of first-order importance in this time scale.

3.2. Relationship with known modes - Covariability between PDO and NAM

In this section, we interpret BCS in the context of known climate modes. Because BCS is associated with the meridional migrations of the atmospheric jet stream, we have performed the Singular Value Decomposition (SVD) between SST and zonal wind anomalies (also known as the Maximum Covariance Analysis). The spatial pattern of the first SVD mode (SVD1) (Fig. 2a) resembles well with that of BCS shown in Fig. 1d. By projecting the original data onto the SVD1 spatial patterns, two SVD1 time series of SST and zonal wind are obtained (Fig. 2d, red and blue curves), whose covariance is maximized due to the SVD definition. In our case, the two SVD1 time series explain 46% of the variances of each other, so our data matrices are suitable for performing SVD.

Our SVD result supports the notion that BCS can be viewed as the covariability shared by PDO and NAM. The

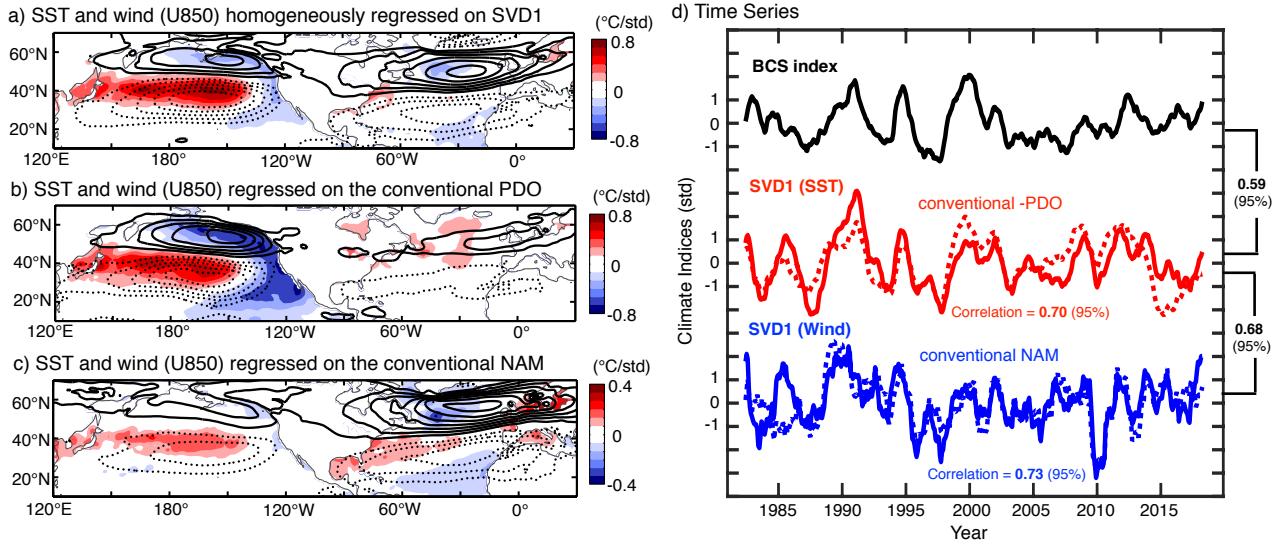


Figure 2. (a): As in Fig. 1d, but homogeneously regressed on the SVD1 time series. (b): As in Fig. 1d, but for the conventional PDO index. (c): As in Fig. 1d, but for the conventional NAM index. (d): Black, As in the black curve in Fig. 1b, but 1-year running meaned. Red solid, SST time series of the first mode of the Singular Value Decomposition (SVD1) calculated between SST and zonal wind at 850 hPa. Red dashed, The 1-year running meaned, conventional Pacific Decadal Oscillation (PDO) index. Blue solid, As in red solid, but for zonal wind at 850 hPa. Blue dashed, The 1-year running meaned, conventional Northern Annular Mode (NAM) index.

SVD1 time series of SST exhibits a correlation of 0.70 with the conventional PDO index (Fig. 2d, red). The SST component of SVD1 explains the low frequency of PDO but also has high covariance with SST at the Gulf Stream (Fig. 2b). On the other hand, the SVD1 time series of zonal wind exhibits a correlation of 0.73 with the conventional NAM index, which is statically significant at the 95 % confidence level (Fig. 2d, blue). The zonal wind component of SVD1 explains the low frequency of NAM but also exhibits high covariance with the midlatitude SST (Fig. 2c).

PDO and NAM are conventionally defined as the first mode of the Empirical Orthogonal Function (EOF) performed for SST and geopotential height, respectively. These definitions purely capture the statistical properties of the climate variables and do not necessarily reflect their physics. Therefore, some arbitrariness remains in how to define these physical modes. Our analysis shows that physically similar modes of climate variability can also be extracted using SVD, and they explain as much as 46% of variances of each other. Based on this evidence, we could speculate that PDO and NAM are related more than previously thought, and that BCS may serve as the key to uncover the relationship of the two conventional climate modes. This view is consistent with previous studies [e.g., Newman *et al.*, 2016] that suggest that the internal PDO variability in the North Pacific are physically separable from the PDO variability forced by the tropical teleconnections.

3.3. Alternative view - the Oceanic Annular Mode

In this section, we further interpret the physical meaning of SVD1 obtained in the previous section. First, it is robust that the SVD1 time series of zonal wind physically means the meridional migrations of the atmospheric jet stream. If we define an index to represent the meridional difference of the regional-mean zonal wind in the manner of the subtropics (45°N-55°N, 120°E-0°W) minus the extratropics (45°N-55°N, 120°E-0°W), this index exhibit a correlation of 0.84 (significant at 95 %) with the SVD1 time series of zonal wind (Fig 3a, bottom). This result is consistent with the

physical interpretation that NAM is a mode that represents meridional migrations of the atmospheric jet stream. In the same manner, if we also define an index to represent the meridional SST difference for the same regions, this index exhibit a correlation of 0.79 (significant at 95 %) with the SVD1 time series of SST (Fig 3a, top). Therefore, SVD1 of SST also describes meridional migrations of SST anomalies.

This SVD result serves as an observational evidence that meridional migrations of the atmospheric jet stream and SST tend to be in phase over the northern hemispheric mid-latitudes. Hence, compared to the conventional view, it is simpler to understand that BCS is an annular mode in the ocean, which we refer to as the Northern Oceanic Annular Mode (NOAM). In other words, there exists a zonally-symmetric midlatitude SST variability that strides over the North American continent. This variability is observable even in the raw SST data, particularly clearly in the western boundaries of the basins, where regional-scale degrees of freedom remains due to the Earth's rotation. The regression map of SST and zonal wind on the NOAM index also captures the BCS variability (Fig. 3b).

If BCS is an oceanic annular mode, it is natural to look for a similar mode in the southern hemisphere. In fact, the Brazil current and the Agulhas return current are also synchronized (Fig. S2), and we could refer to it as the Southern Oceanic Annular Mode (SOAM). Nevertheless, if we perform the same SVD analysis for the southern hemisphere, SOAM is found to be inseparable from the tropical variability, which is in contrast to NOAM, whose signal is confined to the midlatitudes. The evidence that NOAM exhibits the midlatitude internal variability and that SOAM is associated with the tropical forcings is consistent with the feature that SOAM has 3-8 year time scales analogous to the El Niño Southern Oscillation.

A major open question about NOAM is the relationship with NAM. Specifically, it is uncertain whether (i) NOAM is purely a forced response to NAM or (ii) NOAM and NAM form an air-sea coupled mode. Our traditional view is to assume that midlatitude ocean is mostly passive to the atmosphere, but we should not rule out the existence of an

air-sea coupled system for the global and decadal scales. For example, even some early efforts found a hint of air-sea couplings between the storm track and the northern hemispheric WBCs [e.g., *Hoskins and Valdes*, 1990]. Based on more recent evidence, according to *Ogawa et al.* [2012], the meridional position of the eddy-driven jet can be locked by the SST front. Using semi-idealized atmospheric general circulation models, *Omran et al.* [2019] also showed that forcings from both Kuroshio and Gulf Stream are necessary to maintain the wintertime hemispheric circulation and the NAM variability. Furthermore, many previous studies on PDO suggests that oceanic internal variability play an active role at least for decadal time scales. It will be an important next step to investigate whether our climate system forms the “interactive Annular Mode (iAM)” by combining NAM and NOAM.

3.4. Implications for the midlatitude extreme weather and climate change

If BCS plays an active role to determine the low-frequency behavior of the atmospheric jet stream, BCS have some implications for the midlatitude extreme weather. In this section, we take an example from the northern hemispheric hot summer in July 2018 and investigate the relationship with the high SST in the Gulf Stream and the Kuroshio regions.

The spatial pattern of surface temperature anomalies observed in July 2018 (Fig. 4a) corresponds well to the regression map of 2-meter air temperature anomalies on the BCS index calculated using the July-only data (Fig. 4b). East Asia, the west and east coasts of North America, Europe, and Northwest Africa have experienced a hot summer

in 2018, and the BCS index explains these features. As mentioned in the previous section, we have two possible interpretations for this figure. The first interpretation, based on the traditional view that midlatitude ocean is mostly passive to the atmosphere, is that the position of the jet stream determined both the SST and air temperature patterns. In this case, NAM is the cause and NOAM is the effect. As an alternative hypothesis, however, we could also interpret that the position of the jet stream and SST (i.e., NAM and NOAM) has chosen this particular spatial pattern by forming an air-sea coupled mode.

Though more work is needed to confirm the robustness, if this alternative view is plausible, our understanding on the midlatitude jet, and thereby the midlatitude extreme weather and climate change, will be improved by investigating BCS and NOAM. In fact, BCS also gives a consistent explanation for two typical global warming responses: the western boundary currents warm faster than the global mean, and the atmospheric jet stream shifts poleward.

In Fig. 4c, the synchronization between NOAM and 2-meter temperature is also shown in the form of time series. Here, the NOAM index is defined as the SST meridional difference following the previous section, and the 2-meter temperature time series is defined as the projection onto the NOAM regression map of 2-meter temperature. Moreover, these time series also synchronize with the surface temperature projected onto its pattern of July 2018, which means that the extent to which the spatial temperature pattern is

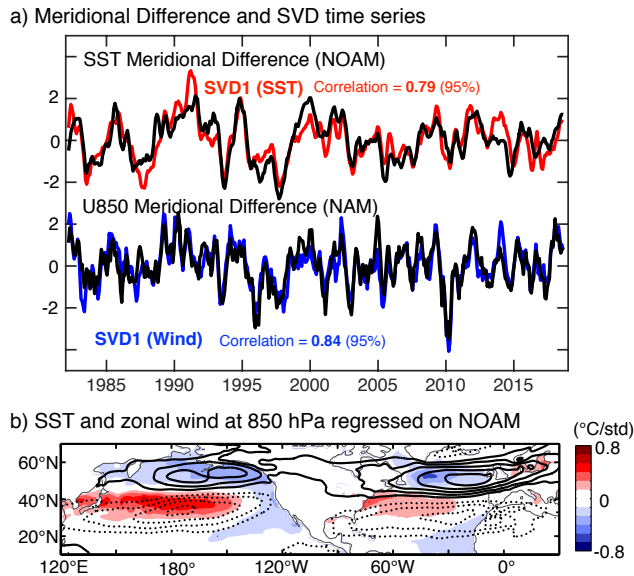


Figure 3. (a): Top black, NOAM index defined as the meridional difference of the regional-mean SSTs calculated in the manner of the subtropics (45°N - 55°N , 120°E - 0°W) minus the extratropics (45°N - 55°N , 120°E - 0°W). 5-month running mean is performed. Red, As in Fig. 2d red solid, but 5-month running-mean time series. Bottom black, NAM index defined as in top black, but for zonal wind at 850 hPa. Blue, As in Fig. 2d blue solid, but 5-month running-mean time series. (b) As in Fig. 1d, but for the NOAM index.

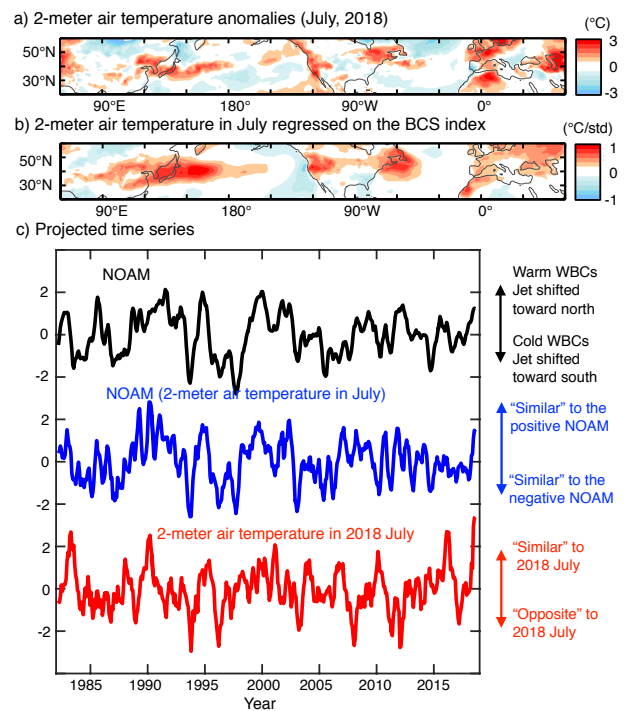


Figure 4. (a): Monthly-mean surface temperature anomalies for July 2018. (b): 2-meter air temperature anomalies in July regressed on the BCS index calculated using the July-only data. (c): Black, As in the top black curve in Fig. 3a. Blue, 2-meter temperature projected on the NOAM spatial pattern (the regression map of 2-meter temperature on the NOAM index). Red, 2-meter air temperature projected on (a).

similar to July 2018 is explained well by NOAM. Considering the short memory of the atmosphere, it appears reasonable to suspect the existence of the air-sea coupled mechanisms to explain the synchronization for interannual time scale.

Our preliminary analysis shows that the result described in the previous paragraph is also true for July 2018 precipitation. This evidence also raises two possible hypotheses: the position of the atmospheric jet stream determines SST and the precipitation pattern, or the atmospheric jet stream and SST form an air-sea coupled system that favors this precipitation pattern. This uncertainty is another reason why we should determine whether NAM and NOAM are coupled.

4. Concluding Remarks

Our view of BCS hypothesizes the existence of an air-sea coupled annular mode, which is analogous to well-known NAM driven by the atmospheric intrinsic variability. However, though many previous studies convincingly showed possible physical processes of interactions between large-scale tropospheric winds and WBCs [Nakamura et al., 2015; Seager et al., 2001; Nonaka and Xie, 2003; Kelly et al., 2010; Ma et al., 2016], our understanding about the mechanism of BCS is limited. Further theoretical considerations, case studies, statistical analyses, and climate model simulations are needed to determine whether our hypothetical view is plausible. In particular, high resolution ocean models will help reveal essential processes of BCS, because they simulate latent heat release from the WBCs better than models with coarser ocean.

At the beginning of this century, a possibly-related theoretical work was presented by Gallego and Cessi [2001]. They developed an idealized model of two ocean basins, each having its own WBC, whose stream function is determined through the time-dependent Sverdrup-balance. In their model, the two WBCs are coupled to each other only through the zonally-symmetric atmosphere. Their model illustrates possible mechanisms of decadal WBC variability via wind-driven torques and heat fluxes, and theoretically predicts the existence of three possible regimes regarding decadal WBC variability. In particular, it is notable that their “chaos” regime exhibits BCS-like variability, but in longer time scale.

As to data analyses, revisiting earlier works on the so-called “Aleutian and Icelandic Lows (AL-IL) Seesaw” [Honda and Nakamura, 2001] may facilitate beginning further investigations of the atmospheric signatures of BCS. To understand the energetic constraints of BCS, relative importance of wind-driven oceanic advections and surface heat fluxes should be thoroughly assessed, following previous studies that investigated the individual WBCs and their extension regions [Vivier et al., 2002; Dong and Kelly, 2004].

Understanding BCS have immediate implications for human lives because BCS modulates the probability of extreme weather events [Sanders, 1986; Young and Sikora, 2003; Minobe et al., 2008] and fisheries productions [Pershing et al., 2015; Watanabe et al., 1996; Saitoh et al., 1986; Tian et al., 2003]. The hot summer experienced in 2018 is a good example of extreme weather associated with BCS. In particular, because other prominent climate modes (e.g., the El Niño Southern Oscillation) were relatively inactive in 2018, the BCS signature may have clearly emerged in the observed air temperature over the entire northern hemispheric extratropics (Fig. 4). As to the fisheries productions, warm SST associated with a northward shift of the Gulf Stream increases the mortality of Atlantic cod (*Gadus morhua*) [Pershing et al., 2015], while migrations of pelagic fish, such as Japanese sardine (*Sardinops melanostictus*) [Watanabe et al., 1996] and Pacific saury (*Cololabis saira*) [Saitoh et al., 1986; Tian et al., 2003], are influenced by the Kuroshio variability because they use the Kuroshio region as spawning and nursery grounds [Kuroda et al., 2016].

Acknowledgments. This work is supported by the Japan Society for the Promotion of Science (JSPS)-Kakenhi Grant Number 19K23460. The second author is supported by JSPS-Kakenhi Grant Number 16H04048. The third author is supported by JSPS-Kakenhi Grant Number 17J04384. We would like to thank Shoshiro Minobe, Yukio Masumoto, Tomoki Tozuka, Masahiro Watanabe, and Yoko Yamagami for useful discussion.

References

- Bretherton, C. S., M. Widmann, V. P. Dymnikov, J. M. Wallace, and I. Bladé (1999), The effective number of spatial degrees of freedom of a time-varying field, *J. Climate*, 12(7), 1990–2009.
- Dee, D. P., S. M. Uppala, A. Simmons, P. Berrisford, P. Poli, S. Kobayashi, U. Andrae, M. Balmaseda, G. Balsamo, d. P. Bauer, et al. (2011), The ERA-Interim reanalysis: Configuration and performance of the data assimilation system, *Quart. J. Roy. Meteor. Soc.*, 137(656), 553–597.
- Dong, S., and K. A. Kelly (2004), Heat budget in the Gulf Stream region: The importance of heat storage and advection, *J. Phys. Oceanogr.*, 34(5), 1214–1231.
- Gallego, B., and P. Cessi (2001), Decadal variability of two oceans and an atmosphere, *J. Climate*, 14(13), 2815–2832.
- Hogg, N. G., and W. E. Johns (1995), Western boundary currents, *Rev. Geophys.*, 33(S2), 1311–1334.
- Honda, M., and H. Nakamura (2001), Interannual seesaw between the Aleutian and Icelandic lows. Part II: Its significance in the interannual variability over the wintertime Northern Hemisphere, *J. Climate*, 14(24), 4512–4529.
- Hoskins, B. J., and P. J. Valdes (1990), On the existence of storm-tracks, *J. Atmos. Sci.*, 47(15), 1854–1864.
- Kelly, K. A., and S. Dong (2004), The relationship of western boundary current heat transport and storage to midlatitude ocean-atmosphere interaction, *Earth’s Climate: The Ocean-Atmosphere Interaction*, *Geophys. Monogr.* 147, 347–363.
- Kelly, K. A., R. J. Small, R. Samelson, B. Qiu, T. M. Joyce, Y.-O. Kwon, and M. F. Cronin (2010), Western boundary currents and frontal air-sea interaction: Gulf Stream and Kuroshio Extension, *J. Climate*, 23(21), 5644–5667.
- Kuroda, H., T. Setou, S. Kakehi, S.-i. Ito, T. Taneda, T. Azumaya, D. Inagake, Y. Hiroe, K. Morinaga, M. Okazaki, et al. (2016), Recent advances in Japanese fisheries science in the Kuroshio-Oyashio region through development of the FRA-ROMS ocean forecast system: Overview of the reproducibility of reanalysis products, *Open J. Marine Sci.*, 7(01), 62.
- Kwon, Y.-O., M. A. Alexander, N. A. Bond, C. Frankignoul, H. Nakamura, B. Qiu, and L. A. Thompson (2010), Role of the Gulf Stream and Kuroshio-Oyashio systems in large-scale atmosphere-ocean interaction: A review, *J. Climate*, 23(12), 3249–3281.
- Ma, X., Z. Jing, P. Chang, X. Liu, R. Montuoro, R. J. Small, F. O. Bryan, R. J. Greatbatch, P. Brandt, D. Wu, et al. (2016), Western boundary currents regulated by interaction between ocean eddies and the atmosphere, *Nature*, 535(7613), 533.
- Mantua, N. J., S. R. Hare, Y. Zhang, J. M. Wallace, and R. C. Francis (1997), A Pacific interdecadal climate oscillation with impacts on salmon production, *Bull. Amer. Meteor. Soc.*, 78(6), 1069–1080.
- Masunaga, R., H. Nakamura, H. Kamahori, K. Onogi, and S. Okajima (2018), JRA-55CHS: An Atmospheric Reanalysis Produced with High-Resolution SST, *SOLA*, 14, 6–13.
- Minobe, S., A. Kuwano-Yoshida, N. Komori, S.-P. Xie, and R. J. Small (2008), Influence of the Gulf Stream on the troposphere, *Nature*, 452(7184), 206.
- Nakamura, H., A. Isobe, S. Minobe, H. Mitsudera, M. Nonaka, and T. Suga (2015), “Hot Spots” in the climate system—new developments in the extratropical ocean-atmosphere interaction research: a short review and an introduction, *J. Oceanogr.*, 71(5), 463–467.

- Newman, M., M. A. Alexander, T. R. Ault, K. M. Cobb, C. Deser, E. Di Lorenzo, N. J. Mantua, A. J. Miller, S. Minobe, H. Nakamura, et al. (2016), The Pacific decadal oscillation, revisited, *J. Climate*, *29*(12), 4399–4427.
- Nonaka, M., and S.-P. Xie (2003), Covariations of sea surface temperature and wind over the Kuroshio and its extension: Evidence for ocean-to-atmosphere feedback, *J. Climate*, *16*(9), 1404–1413.
- Ogawa, F., H. Nakamura, K. Nishii, T. Miyasaka, and A. Kuwano-Yoshida (2012), Dependence of the climatological axial latitudes of the tropospheric westerlies and storm tracks on the latitude of an extratropical oceanic front, *Geophys. Res. Lett.*, *39*(5).
- Omrani, N.-E., F. Ogawa, H. Nakamura, N. Keenlyside, S. W. Lubis, and K. Matthes (2019), Key role of the ocean western boundary currents in shaping the northern hemisphere climate, *Sci. Rep.*, *9*(1), 3014.
- Paul, A., and C. Schäfer-Neth (2003), Modeling the water masses of the Atlantic Ocean at the Last Glacial Maximum, *Paleoceanogr.*, *18*(3).
- Pershing, A. J., M. A. Alexander, C. M. Hernandez, L. A. Kerr, A. Le Bris, K. E. Mills, J. A. Nye, N. R. Record, H. A. Scannell, J. D. Scott, et al. (2015), Slow adaptation in the face of rapid warming leads to collapse of the Gulf of Maine cod fishery, *Science*, *350*(6262), 809–812.
- Reynolds, R. W., T. M. Smith, C. Liu, D. B. Chelton, K. S. Casey, and M. G. Schlax (2007), Daily high-resolution-blended analyses for sea surface temperature, *J. Climate*, *20*(22), 5473–5496.
- Saitoh, S.-i., S. Kosaka, and J. Iisaka (1986), Satellite infrared observations of Kuroshio warm-core rings and their application to study of Pacific saury migration, *Deep Sea Res. Part A. Oceanogr. Res. Pap.*, *33*(11-12), 1601–1615.
- Sanders, F. (1986), Explosive cyclogenesis in the west-central North Atlantic Ocean, 1981–84. Part I: Composite structure and mean behavior, *Mon. Wea. Rev.*, *114*(10), 1781–1794.
- Seager, R., Y. Kushnir, N. H. Naik, M. A. Cane, and J. Miller (2001), Wind-driven shifts in the latitude of the Kuroshio–Oyashio Extension and generation of SST anomalies on decadal timescales, *J. Climate*, *14*(22), 4249–4265.
- Tian, Y., T. Akamine, and M. Suda (2003), Variations in the abundance of Pacific saury (*Cololabis saira*) from the north-western Pacific in relation to oceanic-climate changes, *Fisheries research*, *60*(2-3), 439–454.
- Vivier, F., K. A. Kelly, and L. A. Thompson (2002), Heat budget in the Kuroshio Extension region: 1993–99, *J. Phys. Oceanogr.*, *32*(12), 3436–3454.
- Watanabe, Y., H. Zenitani, and R. Kimura (1996), Offshore expansion of spawning of the Japanese sardine, *Sardinops melanostictus*, and its implication for egg and larval survival, *Can. J. Fish. Aquat. Sci.*, *53*(1), 55–61.
- Wills, R. C., T. Schneider, J. M. Wallace, D. S. Battisti, and D. L. Hartmann (2018), Disentangling global warming, multidecadal variability, and El Niño in Pacific temperatures, *Geophys. Res. Lett.*, *45*(5), 2487–2496.
- Yamamoto, M., T. Oba, J. Shimamune, and T. Ueshima (2004), Orbital-scale anti-phase variation of sea surface temperature in mid-latitude North Pacific margins during the last 145,000 years, *Geophys. Res. Lett.*, *31*(16).
- Young, G. S., and T. D. Sikora (2003), Mesoscale stratocumulus bands caused by Gulf Stream meanders, *Mon. Wea. Rev.*, *131*(9), 2177–2191.
- Yu, L., and R. A. Weller (2007), Objectively analyzed air–sea heat fluxes for the global ice-free oceans (1981–2005), *Bull. Amer. Meteor. Soc.*, *88*(4), 527–540.
- Zhang, R. (2008), Coherent surface-subsurface fingerprint of the Atlantic meridional overturning circulation, *Geophys. Res. Lett.*, *35*(20).

Corresponding author: T. Kohyama, Department of Information Sciences, Ochanomizu University, 2-1-1, Otsuka, Bunkyo-ku, Tokyo, 112-8610, Japan. (tsubasa/at/is.ocha.ac.jp)

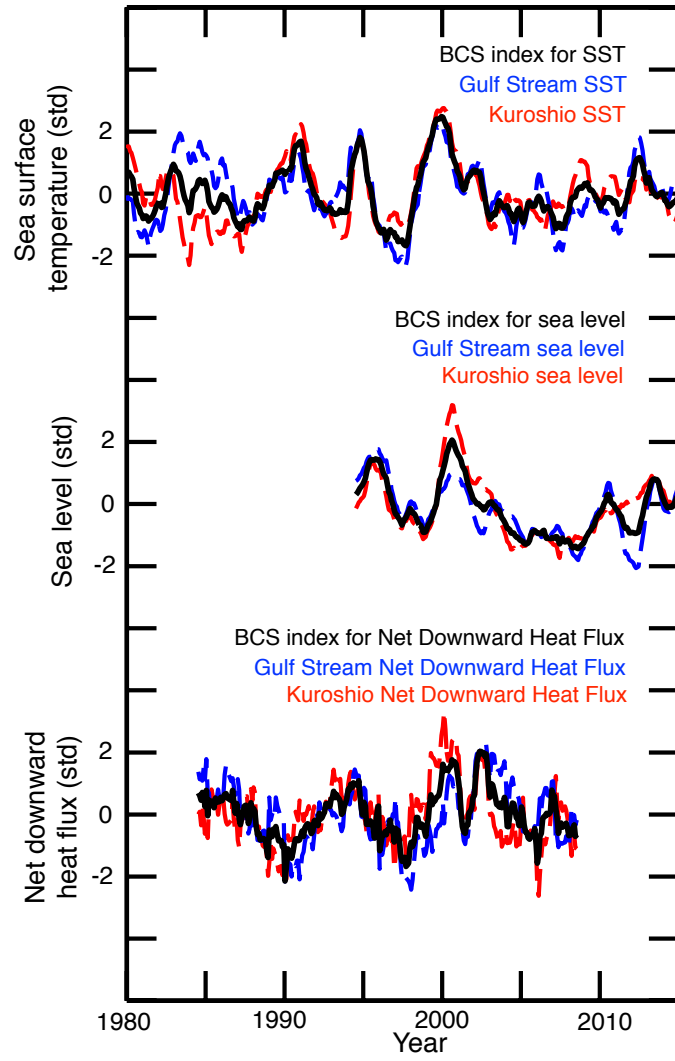


Figure S1. As in Fig. 1b, but with time series of sea level (middle) and net downward surface heat flux (i.e., the total of latent and sensible fluxes at the surface from atmosphere to ocean) (bottom).

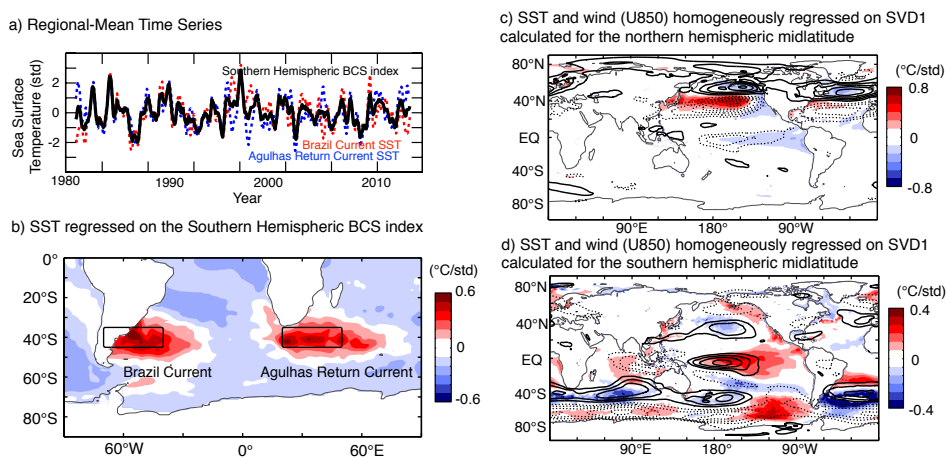


Figure S2. (a): As in Fig. 1b, but for the Southern Hemispheric Midlatitude SST (70°S - 30°S , all longitudes). Boxes show the locations of the two southern hemispheric WBCs. (b): As in the shaded area in Fig. 1c, but for the Brazil Current (35°S - 45°S , 70°W - 40°W) and the Agulhas Return Current (35°S - 45°S , 20°E - 50°E). (c): As in Fig. 2a, but the global map is shown. (d): As in (c), but for the southern hemisphere.